Applied Catalysis B: Environmental 224 (2018) 183–193

Contents lists available at ScienceDirect

Applied Catalysis B: Environmental

journal homepage: www.elsevier.com/locate/apcatb

Tin phosphate as a heterogeneous catalyst for efficient dehydration of glucose into 5-hydroxymethylfurfural in ionic liquid

Qidong Hou, Meinan Zhen, Le Liu, Yu Chen, Fang Huang, Shiqiu Zhang, Weizun Li*, Meiting Ju*

Tianjin Engineering Research Center of Biomass Solid Waste Resources Technology, College of Environmental Science and Engineering, Nankai University, Tianjin 300350, PR China

ARTICLE INFO

Keywords:
5-Hydroxymethylfurfural
Glucose
Heterogeneous catalysis
Dehydration
Ionic liquid

ABSTRACT

5-Hydroxymethylfurfural (HMF) is a key versatile building block in the valorization of lignocellulosic biomass. A series of metal oxides and metal phosphates was investigated as heterogeneous catalyst to convert glucose into HMF in the ionic liquid 1-ethyl-3-methylimidazolium bromide (EMIMBr). The heterogeneous conversion of a high-concentration glucose (up to 20 wt%) into HMF in ionic liquid has been achieved for the first time. Tin phosphate in the medium could afford a high HMF yield (58.3%) comparable to the best results obtained with the most effective homogeneous catalysts. To elucidate the reaction mechanism, SnO_2, sSnPO and SnPO were characterized by N_2 adsorption-desorption, XRD, TEM, XPS, UV–vis, FIIR, Py-IR and CD_3CN-IR. It was found that tetra-coordinated Sn^{4+} sites from tin phosphate are responsible for the isomerization of glucose into fructose, while the conversion of fructose into HMF is mainly catalyzed by the ionic liquid EMIMBr. The excellent catalytic performance was attributed to the synergistic effect between SnPO and EMIMBr.

1. Introduction

To alleviate worldwide problems associated with diminishing fossil fuel resources, tremendous efforts have been focused on the utilization of lignocellulosic biomass [1–5]. Biorefinery technologies have been intensively investigated to convert lignocellulosic biomass into value-added fuels, fine chemicals and materials over the past decade [6–14]. In the biorefinery, the conversion of glucose—the most abundant component in lignocellulosic biomass [15–18]—into 5-hydroxymethylfurfural (HMF) is of great importance [6,19]. As a versatile intermediate, HMF is a critical starting material for the synthesis of other platform chemicals and novel materials to displace fossil resource-derived products [20–29]. For instance, 2,5-furandicarboxylic acid (FDCA), which is synthesized from HMF via oxidation, has been identified as a promising alternative building block for the production of plastics [30–33]. Therefore, it is highly desirable to develop an efficient catalytic process for the production of HMF from biomass [34].

Both homogeneous and heterogeneous catalysis have been attempted to convert glucose into HMF [35]. Several homogeneous catalysts, including $CrCl_3$, $CrCl_3$, $SnCl_4$ and $AlCl_3$, were found to be capable of converting glucose to HMF in some ionic liquids, high boiling point organic solvents and/or biphasic systems [36–42]. Compared with homogeneous catalysis, heterogeneous catalysis has attracted increasing attention in light of catalyst recycling and reuse [35,43]. In biphasic systems consisting of water (or aqueous solutions of salt) and organic solvents that can efficiently separate HMF from water, a series of metal oxides, metal phosphates and partial phosphorylated metal oxides was developed as heterogeneous catalysts for the conversion of glucose into HMF, significantly expanding knowledge of the catalytic conversion of glucose [44–46]. Despite these rapid advances in the development of catalyst, the relatively high yields of HMF obtained from these reaction systems are to a large extent attributed to the successive extraction of HMF from the reaction phase to the organic phase [47]. High temperature is usually needed to promote the dehydration reaction, but harsh conditions will concomitantly accelerate the side-reactions, including the decomposition of HMF into levulinic acid and formic acid and the formation of humins [35]. Therefore, although the conversion of glucose into HMF in aqueous biphasic systems has been widely investigated using various catalysts, unrealistic reaction conditions—including high catalyst loading, high reaction temperature, long reaction time, low substrate loading, and large amounts of extraction solvents and salts that could deliver HMF from the reaction phase to the extraction phase—are required to obtain high glucose conversion and HMF selectivity [34]. Therefore, a long-term goal in this field is to develop an efficient heterogeneous reaction system that can convert high concentrations of glucose into HMF selectively under relatively mild conditions [37].

It is generally believed that the conversion of glucose into HMF

* Corresponding authors.
E-mail addresses: liweizun@nankai.edu.cn (W. Li), jumeit@nankai.edu.cn (M. Ju).

http://dx.doi.org/10.1016/j.apcatb.2017.09.049
Received 6 July 2017; Received in revised form 19 September 2017; Accepted 22 September 2017
Available online 22 September 2017
0926-3373/

includes two steps: isomerization of glucose into fructose and dehydration of fructose into HMF. The isomerization of glucose into fructose can be catalyzed by some Lewis acid sites and some alkaline sites, but fructose selectivity is low in most cases, since the increasing equilibrium concentration of fructose retards further conversion of glucose [48,49]. The dehydration of fructose to HMF can be readily achieved in some ionic liquids and aprotic organic solvents using Brφnsted acids, including mineral acids, acidic ionic liquids and a broad range of solid acids, as catalysts [50–54]. In suitable medium, such as the ionic liquids 1-ethyl-3-methylimidazolium bromide (EMIMBr) and 1-butyl-3-methylimidazolium bromide (BMIMBr), fructose can be converted into HMF almost quantitatively in the absence of additional catalyst [55]. Therefore, we inferred that the combined employment of ionic liquid EMIMBr and catalysts that are active for the isomerization of glucose into fructose may enable the efficient conversion of glucose into HMF through one-pot reaction. In a previous study, we have preliminarily demonstrated this concept. We found that $SnCl_4$ dissolved in EMIMBr could efficiently convert high-concentration glucose into HMF. Even at a very high glucose loading (glucose/EMIMBr weight ratio = 1), the HMF yield still reached 40%. However, efficient HMF production using heterogeneous catalyst in ionic liquid has not been achieved in practice, to the best of our knowledge [34,35]. The search for heterogeneous catalysts, especially those that are highly selective and active in ionic liquids and can be readily recycled, is vital for the development of sustainable chemical processes for the efficient production of HMF from biomass [34]. The catalytic conversion of glucose in water and aqueous biphasic systems has been well established, providing a wealth of potential catalysts which may be effective in ionic liquids [35].

In this work, we prepared a series of metal oxides and metal phosphates as heterogeneous catalysts for the dehydration of glucose into HMF in ionic liquid. The influence of temperature, time, organic solvent, and catalyst on HMF yields was investigated to optimize the experimental conditions for HMF production. The role of catalyst and ionic liquid was illustrated via characterization of the catalyst and control experiments.

2. Experiment

2.1. Materials and reagents

Fructose (99%), glucose (99%), 5-hydroxymethylfurfural (99%), $SnCl_4{\cdot}5H_2O$, glycol dimethyl ether (GDE, 99%), dimethyl formamide (DMF, 99%), dimethyl acetamide (DMAc, 99%), dimethyl sulfoxide (DMSO, 99%), P 25, Rutile TiO_2 (R- TiO_2), and Anatase TiO_2 (A-TiO_2) were purchased from Tianjin Heowns Biochem LLC (Tianjin, China). Ionic liquids, including 1-allyl-3-methylimidazolium chloride (AMIMCl, 99%), EMIMCl (99%), BMIMCl (99%), EMIMBr (99%) and BMIMBr (99%), were purchased from Shanghai Chengjie Chemical Reagent Co. Ltd., China. Another $EMIMBF_4$ (99%) product was obtained from Lanzhou Zhongkekaite Co. Ltd., China. All the other chemical reagents were purchased from commercial sources in China and used as received.

2.2. Catalyst preparation and characterization

Tin phosphate was synthesized by adapting a previously described method [56]. P123 (1 g) and H_3PO_4 (1.15 g, 10 mmol) were dissolved in H_2O (15 g), and this mixture was stirred for 2 h. $SnCl_4{\cdot}5H_2O$ (3.5 g, 10 mmol) dissolved in H_2O (5 g) was added to the H_3PO_4 solution. A white colloidal precipitate formed slowly. The mixture was stirred for another 3 h and kept in a polypropylene bottle at 100 °C for 72 h. The white material was collected by filtration and washed with water and ethanol five times, respectively. The obtained solid was dried at ambient temperature and calcined at 700 °C for 5 h. The calcined sample was labeled as SnPO. Other metal phosphates, including AlPO, TiPO, CrPO, FePO, ZrPO and NbPO were synthesized according to the above method [45,57]. Besides, a small pore tin phosphate was synthesized according to the above procedure without using P123 and labeled as sSnPO.

The surface morphology of catalyst was analyzed by a Tecnai G2 F20 S-TWIN high resolution transmission electron microscope (FEI, America). The N_2 adsorption/desorption isotherms were measured at 196 °C on an automatic ASAP 2460 system from Micromeritic. Before the measurements, the catalyst was degassed at 250 °C in vacuum for 6 h. The powder X-ray powder diffraction (XRD) patterns were measured by a X'pert MFD diffractometer using Cu-Kα radiation (λ = 1.5406 Å) generated at a voltage of 40 kV and a current of 40 mA. Scans were obtained from 2θ = 5–70° at a scanning rate of 5° min^{-1}. The Fourier transform infrared (FTIR) spectra were recorded using a FTS 6000 FTIR spectrometer (Bio-rad, USA). The test samples were prepared using KBr-disk method. The spectra were measured from 4000 to 400 cm^{-1} at a resolution of 2 cm^{-1} in the transmission mode. The coordination state of tin was probed by UV–vis diffuse reflectance spectroscopy. Spectra were recorded on a Shimadzu UV-3600 spectrophotometer using $BaSO_4$ as reference. X-ray photoelectron spectra were recorded using a ESCALAB 250Xi X-ray Photoelectron Spectrometer (Thermo Fisher Scientific, America). A PHI ACCESS ESCA-V6.0 F software package was used for data analysis. A Shirley-type background was subtracted from the signals. All recorded spectra were fitted using Gaussian-Lorentzian curves to more accurately determine the binding energy of the different element core levels. To probe the surface acid sites, the pyridine adsorption FTIR spectra (Py-IR) and deuterated acetonitrile adsorption FTIR spectra (CD_3CN-IR) were collected on a Bruker TENSOR 27 spectrometer by averaging 64 scans at resolution of 2 cm^{-1} in the 4000–400 cm^{-1} range. The spectra were taken relative to an empty cell background reference collected under dynamic vacuum (rotary vane rough pump, Alcatel 2008A, < 0.1 Torr) at 150 °C for pyridine and 30 °C for CD_3CN, respectively. The powder samples were pressed into translucent disks, degassed in vacuum at 400 °C for 2 h, and then cooled down to the desired temperature under dynamic vacuum. The sample was cooled to 150 °C for adsorption experiments with pyridine, or to 30 °C for adsorption experiments with CD_3CN, and then exposed to pyridine or CD_3CN vapor. When samples reached equilibrium with a detectable gaseous pressure (0.4–2.0 Torr), samples were exposed to dynamic vacuum for 30 min (at 303 K for CD_3CN or at 423 K for pyridine) to remove gas-phase and weakly-bound species. The Py-IR spectra and CD_3CN-IR spectra were then recorded at 150 °C and 30 °C, respectively.

2.3. Catalytic tests

Catalytic tests were performed in 10-mL closed thick-walled glass reactors, which were placed in an oil bath and heated at 120 °C with magnetically stirring. Known amounts of glucose and catalyst were added to ionic liquid or a biphasic system consisting of ionic liquid and organic solvent. The catalyst/glucose weight ratio was set as 0.50 unless specifically stated. The mixture was stirred at a fixed temperature for the desired time after which the reactor was cooled to room temperature in a cold-water bath and diluted with water (for pure IL) or methanol (for the biphasic system). The sample was filtered with a 0.45-μm polytetrafluoroethylene filter membrane to remove insoluble solid. The concentration of HMF was measured at 284 nm with high-performance liquid chromatography (HPLC) equipped with a diode array detector (DAD). The concentration of glucose and fructose was measured with an HPLC equipped with an evaporative light scattering detector (SofTA, ELSD Model 300s) and a Xtimate ®Sugar-Ca analytical column (7.8 × 300 mm, 5 μm). The column oven temperature was set to 80 °C, and the mobile phase was ultrapure water at a flow rate of 0.50 mL/min. The glucose conversion, HMF yield and selectivity were calculated according to the following equations:

$$\text{Glucose conversion (mol\%)} = \frac{(\text{moles of starting glucose} - \text{moles of remaining glucose})}{\text{moles of starting sugar}} \times 100\% \quad (1)$$

$$\text{HMF yield (mol\%)} = \frac{\text{moles of produced HMF}}{\text{moles ofstarting glucose}} \times 100\% \quad (2)$$

$$\text{HMF selectivity (mol\%)} = \frac{\text{moles of produced HMF}}{(\text{moles of starting glucose} - \text{moles of remaining glucose})} \times 100\% \quad (3)$$

The catalytic performance of the reaction system was evaluated by observing the conversion of glucose and the selectivity and yield of products. All results were replicated at least three times, and the reproducibility of glucose conversion, HMF yield and HMF selectivity were within 3% standard deviation.

2.4. Filtration test

For the filtration test, original SnPO was added to fresh EMIMBr and heated for 3 h at 120 °C. The obtained suspension was diluted with anhydrous ethanol and then filtered to separate the catalyst and ionic liquid. The recovered catalyst was dried for 24 h at 80 °C under vacuum and added to fresh ionic liquid for the catalytic reaction. The ethanol in the filtered liquor was removed by distillation to obtain ionic liquid, which may contain dissociated ions. The recovered ionic liquid was also used for the catalytic reaction to evaluate the possible impact of dissociated ions from catalyst.

2.5. Recycling experiments

After the first run, the reaction mixture was diluted with water. The catalyst containing insoluble humins was separated from the ionic liquid through filtration. The catalyst was washed with water and ethanol to remove most adsorbed species. The recovered catalyst was dried for 24 h at 80 °C under vacuum (−0.098 Mpa) and directly reused in the next catalytic run without calcination. In subsequent runs, the catalyst was calcined at 973 K for 5 h prior to reuse, in order to remove humins and reactivate the catalyst. The experimental parameters (reaction time, temperature, glucose loading) were the same as the initial catalytic test.

3. Results and discussion

3.1. Catalytic study

3.1.1. Screening of catalysts for conversion of glucose to HMF

A series of metal oxides and metal phosphates were tested for the dehydration of glucose to HMF at 120 °C for 3 h in EMIMBr, using a glucose loading of 10 wt% with respect to EMIMBr. The glucose conversion, HMF yield and selectivity are shown in Fig. 1. In these catalysts, SnPO exhibited both high glucose conversion and HMF yield. Although AlPO, TiPO, ZrPO, and NbPO showed high glucose conversion between 89 and 100%, HMF yields were between 27.5 and 30.6%, with HMF selectivity near 30%. Other metal phosphates including FePO and CrPO showed lower glucose conversions and lower HMF yields. The poor catalytic performance of CrPO indicated that the PO_4^{3-} anion is not the active site for the conversion of glucose, since free Cr^{3+} ion is very active for this conversion [36,58]. Interestingly, some metal oxides were found to be capable of catalyzing the conversion of glucose in EMIMBr. The commercially available TiO_2 products P 25 and A-TiO_2 (anatase) exhibited considerable glucose conversion with HMF yields of 13.8% and 10.9%, respectively. In contrast, R-TiO_2 (Rutile) showed both insufficient glucose conversion and low HMF yield. The obvious

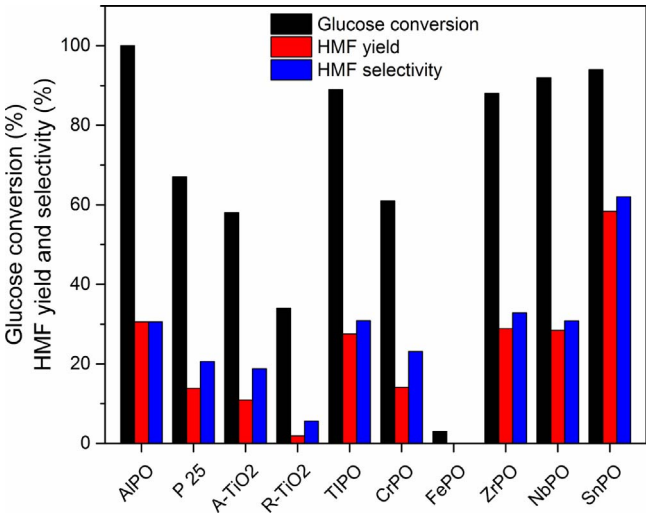

Fig. 1. Effect of catalysts on dehydration of glucose into HMF in EMIMBr. Conditions: 100 mg sugar dissolved in 1000 mg of EMIMBr; mass ratio of catalyst: glucose = 1:2; 120 °C; 3 h.

catalytic activity of metal oxides also supported the hypothesis that the catalytic sites are metal species, not PO_4^{3-} anion.

Since SnPO are the most active catalyst, other Sn containing materials including SnO_2 and sSnPO were prepared and tested for the conversion of glucose to identify the active sites. As shown in Fig. 2, both glucose conversion and HMF yield increased in the order: SnO_2 < sSnPO < SnPO. It should be noted that the catalysts after calcination treatment showed obvious higher glucose conversion and HMF yield than the corresponding catalysts without calcination treatment. The influence of catalyst loading on the conversion of glucose was also investigated. As shown in Fig. 3a, the maximal HMF yield increased remarkably when the catalyst/glucose weight ratio increased from 0.10 to 0.50. When the catalyst/glucose weight ratio was less than 0.15, and the initial HMF formation rate increased linearly with the increase of catalyst loading (Fig. 3b). However, the further increase of catalyst/glucose weight ratio from 0.50 to 1.00 could slightly increase the initial HMF formation rate but could not improve the maximal HMF yield. Besides, when the loading of catalyst was constant, the initial HMF formation rate increased remarkably with the increase of glucose

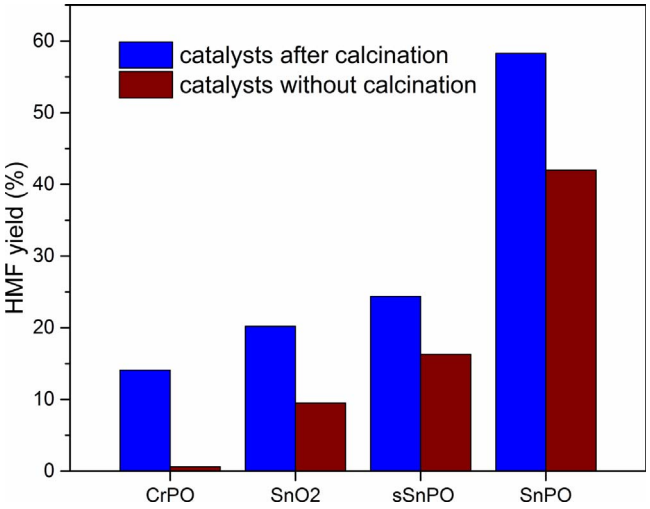

Fig. 2. Comparison of catalysts before and after calcination for dehydration of glucose into HMF in EMIMBr. Conditions: 100 mg sugar was dissolved in 1000 mg of EMIMBr; mass ratio of catalyst: glucose = 1:2; 120 °C; 3 h.

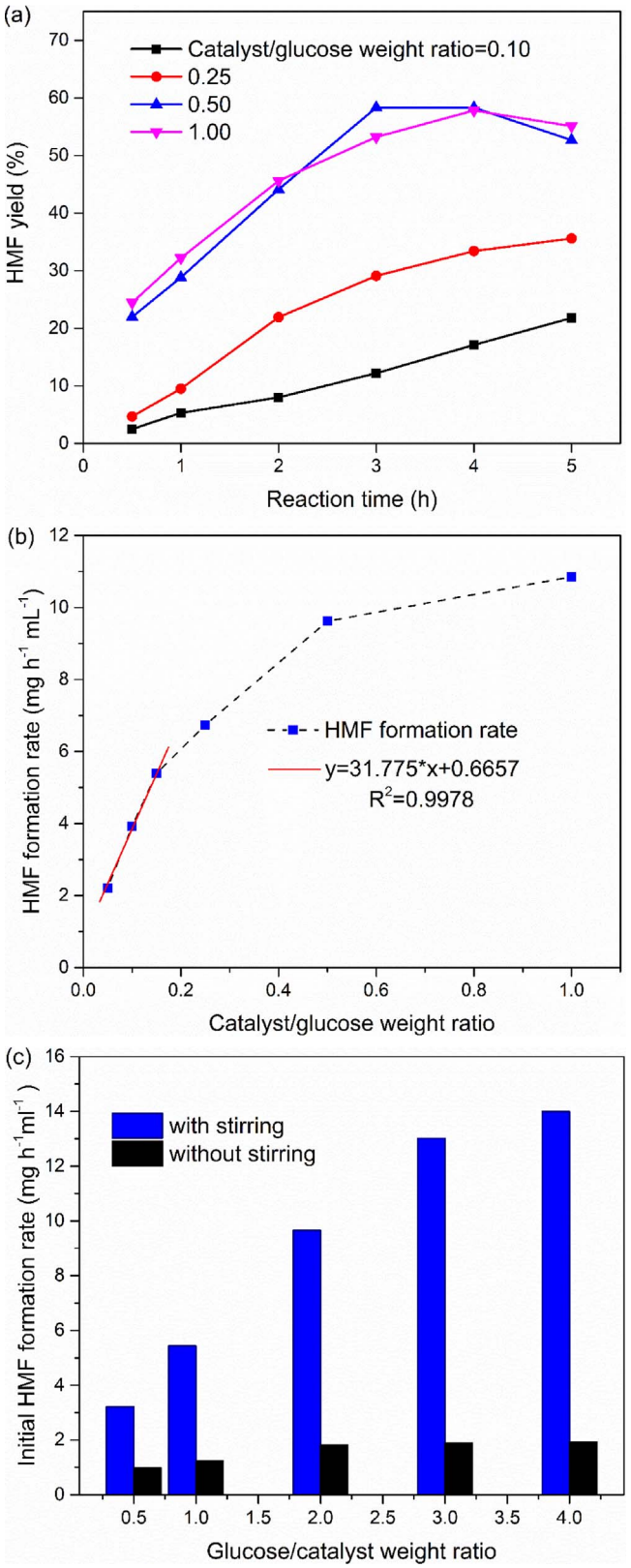

Fig. 3. Effect of catalyst loading on HMF yield (a) and initial HMF formation rate (b) using a constant glucose loading (100 mg). Effect of glucose loading on initial HMF formation rate (c) using a constant catalyst loading (50 mg).

loading (Fig. 3c). Moreover, the initial HMF formation rate reduced obviously when the reaction was performed without stirring. These results suggest that the reaction is not controlled by mass transfer at low catalyst loading, and may be influenced by mass transfer at high catalyst loading.

Table 1
Effect of solvent on conversion of glucose into HMF.

Entry	Solvent	t (h)	Yield of HMF (%)	Yield of fructose (%)
1	EMIMBr	3	58.3	< 1
2	BMIMBr	3	57.1	< 1
3	EMIMCl	3	16.9	< 1
4	BMIMCl	3	17.3	< 1
5	AMIMCl	3	15.8	< 1
6	DMF	5	6.7	< 1
7	DMAC	5	18.2	< 1
8	DMSO	5	24.2	< 1
9	water	5	5.1	6.3
10	EMIMBr/GDE[a]	3	43.3	< 1

Reaction conditions: glucose was reacted at 120 °C at a concentration of 10 wt% relative to the total mass of solvent; mass ratio of catalyst: glucose = 1:2.

[a] A biphasic solvent system consisting of 20 wt% EMIMBr and 80 wt% GDE was used as reaction medium; glucose was reacted at 120 °C at a concentration of 10 wt% relative to the total mass of EMIMBr and GDE; mass ratio of catalyst: glucose = 1:2.

3.1.2. Effect of solvent on conversion of glucose to HMF

The effect of solvent on the conversion of glucose to HMF using SnPO as catalyst was investigated. As shown in Table 1, the HMF yield obtained with BMIMBr was comparable to that obtained with EMIMBr. Although EMIMCl, BMIMCl, AMIMCl, DMF, DMAc and DMSO, have been widely used as reaction media for the conversion of glucose and fructose into HMF in previous studies, they give remarkably lower HMF yields when using SnPO as catalyst. When water was used as reaction medium, the HMF yield was only 5.1%. Interestingly, fructose was also formed in water. In contrast, fructose was not detected in other solvents owing to the rapid conversion of fructose in these solvents. The yield of fructose (6.3%) obtained with SnPO in water was considerably lower than that obtained with Sn-beta zeolite [59]. The poor activity of SnPO in water was attributed to the lack of hydrophobicity of SnPO [60]. An HMF yield up to 43.3% was obtained from the EMIMBr/GDE biphasic system, consisting of 20 wt% EMIMBr and 80 wt% GDE. After reaction GDE extracted approximate 60% of the formed HMF from EMIMBr. Owing to the relative low boiling point (83 °C) of GDE, HMF and GDE could be readily separated by distilling. This reaction system is very promising for actual application since large amount of ionic liquid was displaced with organic liquid.

3.1.3. Reuse of solid catalyst

To test the recyclability and stability of the reaction system, a recycling experiment was performed. Water plays an important role in the reaction process. On one hand, the water released from reaction process is generally harmful to the dehydration reaction [34]. On the other hand, water has important influences on the catalytic performance of catalyst. Therefore, the catalyst was dried under vacuum to sufficiently remove water. When the catalyst was recovered without calcination, glucose conversion and HMF decreased obviously in the second run (Fig. 4), mainly due to the formation of humins that cannot be removed from the catalyst without calcination treatment. In the subsequent runs, the catalyst was reactivated though calcination prior to reuse. After five runs, the conversion of glucose and the HMF yield still maintained to 92.0% and 56.5%, indicating that the solid catalyst can be reused with slight loss of catalytic activity (Fig. 5). The heterogeneous nature of the reaction system was further confirmed by the following filtration test. In the filtration test, the catalyst was first dispersed in the ionic liquid EMIMBr and treated at 120 °C for 3 h. After this treatment, the catalyst and ionic liquid EMIMBr were recovered. When the recovered catalyst was reused for the conversion of glucose in fresh ionic liquid, HMF yield was comparable to that obtained with fresh catalyst. When the reaction

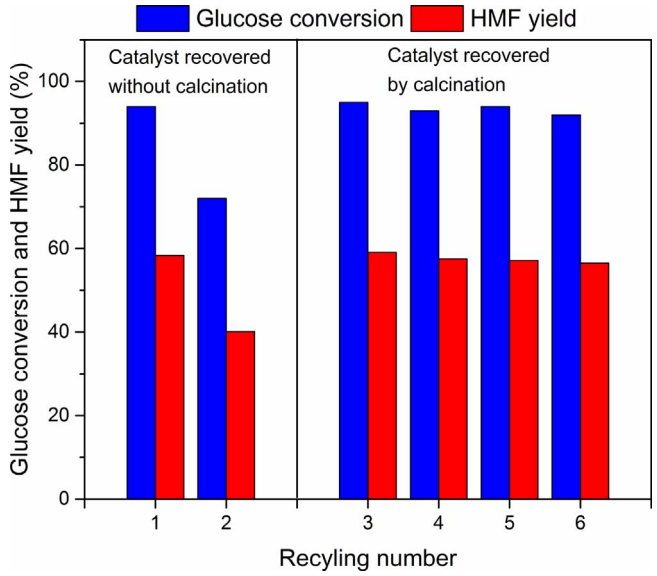

Fig. 4. Recycling of catalyst. In the second run, the catalyst was recovered without calcination. In subsequent runs, the catalyst was recovered by calcination. Reaction conditions: 100 mg sugar dissolved in 1000 mg of EMIMBr; 120 °C.

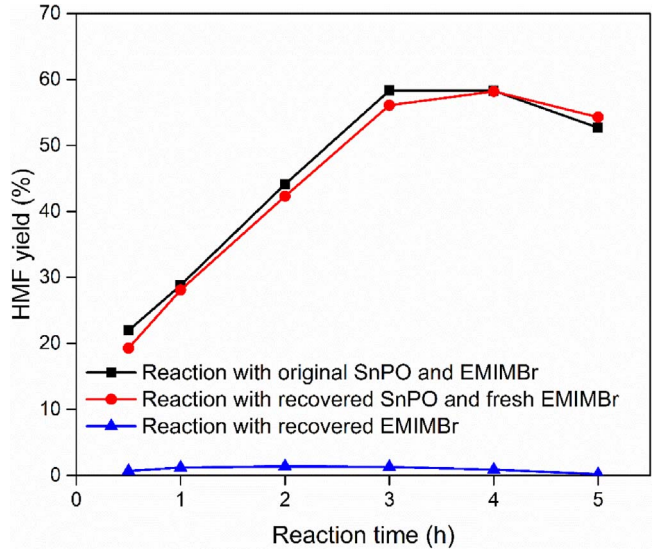

Fig. 5. Results of filtration test. Reaction conditions: 100 mg sugar was dissolved in 1000 mg of EMIMBr; 120 °C.

was performed in the recovered EMIMBr without additional catalyst, HMF yield was less than 2% during the whole reaction process. The recycling experiment and filtration test demonstrated that the reaction using SnPO as catalyst is a true heterogeneous catalytic process.

3.1.4. Comparisons with other catalytic system

The catalytic performance of metal oxides and metal phosphates in ionic liquids was compared with other reaction systems. In comparison with previously reported reaction systems, the use of EMIMBr as an alternative reaction medium to water and aqueous biphasic systems could considerably improve the conversion efficiency of glucose to HMF from multiple perspectives. As shown in Table 2, the HMF yield and selectivity obtained with SnPO/EMIMBr in the present work are significantly higher than the optimal HMF yield and selectivity obtained with other heterogeneous catalytic systems regardless of reaction conditions. The loading of glucose used in the present work is considerably higher than other heterogeneous catalytic systems. When glucose loading up to 20 wt% was used, the HMF yield from the SnPO/EMIMBr system could still reach as high as 52.3%. At the same time, the reaction temperature used in our work is remarkably lower than other heterogeneous catalytic systems. Although water is usually considered an environmental friendly solvent according to principles of green chemistry, the use of large amounts of organic solvent and salt in the biphasic systems will cause environmental issues in practice [59,61]. In summary, the heterogeneous catalytic process using EMIMBr as reaction medium has obvious advantages over previously developed heterogeneous catalytic processes.

Compared with the most efficient homogenous catalytic systems, including $CrCl_3$ dissolved in BMIMCl and $SnCl_4$ dissolved in EMIMBr, the HMF yield from the SnPO/EMIMBr system is slightly lower, and higher reaction temperature and loading of catalyst is required to obtain the maximal HMF yield. However, the heterogeneous catalytic process is still more attractive than the homogenous catalytic processes owing to many advantages, including the facile recovery and reuse of catalysts and the avoidance of environmental pollutions. By combining the advantages of both heterogeneous and homogeneous catalysts, the further development of heterogeneous catalytic processes in ionic liquid may greatly promote environmental friendly and economically viable HMF production.

3.2. Characterization of the catalysts

3.2.1. Physicochemical properties and morphology

TEM images of SnO_2, sSnPO and SnPO are shown in Fig. 6. Both SnO_2 and SnPO, which are prepared using P123 as a structure-directing agent, are composed of small spherical nanoparticles. As expected, sSnPO has much larger particle size than SnO_2 and SnPO. The magnified views of the TEM images of SnO_2 and SnPO also showed internal mesoscopic void space due to particle accumulation. The small particle size and the presence of pores could promote mass transport between catalyst and substrate, thus improving catalytic activity.

As shown in Fig. 7a, the N_2 adsorption/desorption isotherms of SnO_2, sSnPO and SnPO are type IV isotherms with a H4 hysteresis loop at the high relative pressure region. As expected, SnPO and SnO_2 have larger specific surface area than SnO_2 (Table 3). Additionally, Fig. 7b shows that SnO_2 and SnPO have a relatively wide pore diameter distribution between 2 and 30 nm, in accordance with the TEM images.

3.2.2. Catalyst structure and chemical state

As shown in Fig. 8, the XRD pattern of SnPO and sSnPO exhibits one broad peak centered near 22.0°, confirming their amorphous nature [68]. In contrast, the XRD pattern of SnO_2 shows sharp peaks at 2θ = 33.9 and 51.8°, attributed to the d_{101} and d_{211} reflections of bulk SnO_2, respectively [69]. It should be noted that the d_{101} and d_{211} reflections are also visible in the XRD pattern of sSnPO, demonstrating the formation of small amount of SnO_2 in the sSnPO sample.

The FTIR spectra of SnPO, sSnPO and SnO_2 are shown in Fig. 9. The FTIR spectra of SnPO exhibited a very broad band, ranging from 1000 to 1250 cm^{-1} assigned to the asymmetric Sn—O—P stretching vibration, indicating the presence of a phosphate framework. This band shifted from 1124 cm^{-1} for SnPO to 1080 cm^{-1} for sSnPO with slightly lower intensity, suggesting the phosphorylation of sSnPO is insufficient. This is consistent with the XRD analysis and the following measurements, including Diffuse reflectance UV–vis spectroscopy and X-ray photoelectron spectroscopy.

Diffuse reflectance UV–vis (DRUV) spectra of catalysts in dehydrated and hydrated state were measured to probe Sn coordination and detect tetrahedrally-coordinated Sn centers. The DRUV spectrum of dehydrated SnPO (Fig. 10a) showed one sharp peak centered at 203 nm, suggesting the formation of isolated tetrahedrally coordinated Sn^{4+} species in this sample. Since UV–vis is very sensitive for the detection of SnO_2 phases [70], the absence of a UV–vis band near 300 nm

Table 2
Comparisons of catalytic behavior of SnPO in EMIMBr and representative catalytic systems for conversion of glucose to HMF.

Catalyst	Solvent	T (°C)	t (h)	Loading (%)	Conversion (%)	Yield (%)	Selectivity (%)	Ref.
Nb_4W_4	water	120	2	4.5	36.1	18.8	52.1	[62]
Sn-Beta/HCl[a]	water	140	2	10	72.0	11.0	15.3	[61]
γ-Al_2O_3	water/MIBK/$CaCl_2$	175	0.25	3	96	52	54.2	[63]
TaPO	water/MIBK	170	1	3	56.3	32.8	58.3	[64]
Ta_2O_5	water/MIBK	175	1.5	3	69	23	33.3	[65]
Al-MCM[a]	water/MIBK	195	2.5		87	36	41.3	[66]
Nb_2O_5[a]	water	180	0.3	1		36		[44]
TiO_2	water	120	2	1	85	10	12	[67]
$CrCl_3$	EMIMCl	100	3	10	100	45	45	[36]
SnPO	EMIMBr	120	3	10	94.1	58.3	62.0	This work
SnPO	EMIMBr	120	3	20	94.6	52.3	55.3	This work

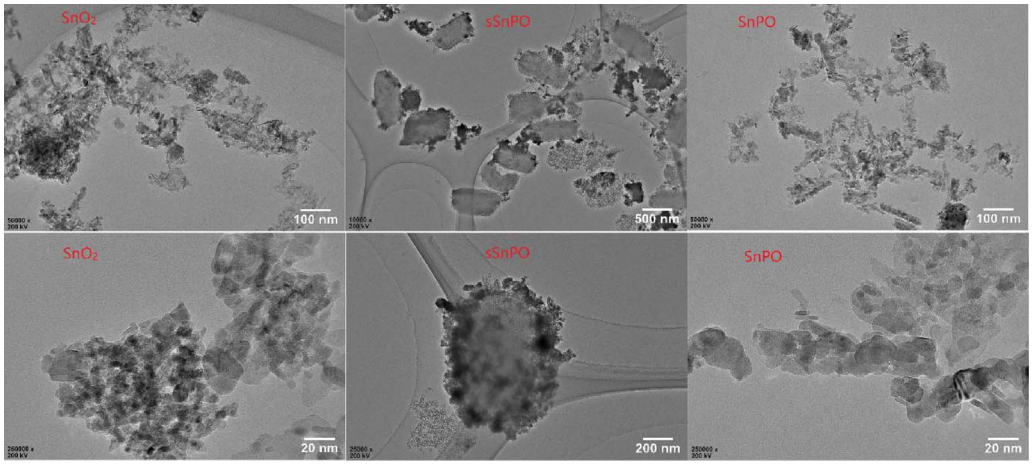

Fig. 6. TEM images of SnO_2, sSnPO and SnPO.

which is attributed to either as an extra-framework SnO_2 phase or a doubly hydrated framework Sn^{4+} single-site species [70], confirmed that no bulk SnO_2 phase was present in the dehydrated SnPO [71]. The DRUV spectrum of dehydrated SnO_2 showed a very broad band ranging from 250 to 300 nm, which was assigned to hexa-coordinated and octahedrally coordinated Sn^{4+} sites. The DRUV spectrum of dehydrated sSnPO showed a broad band ranging from 200 to 250 nm, suggesting the presence of both tetra-coordinated and hexahedrally coordinated Sn^{4+} species. The XRD analysis has demonstrated the presence of small amounts of SnO_2 in the sSnPO samples. Since the UV–vis band centers of small SnO_2 domains also fall in the range of 200–250 nm due to the quantum confinement effect [60,72], the peak at 300 nm assigned to bulk SnO_2 was absence in the dehydrated sSnPO sample. The content of tetrahedrally coordinated Sn^{4+} in SnPO, sSnPO and SnO_2 is highly correlated with their catalytic activity, indicating that tetrahedrally coordinated Sn^{4+} sites are the main catalytic species. After hydration treatment, the DRUV spectra of SnPO, sSnPO and SnO_2 all showed a broad band between 250 and 320 nm (Fig. 10b). These results suggested that the Sn^{4+} sites in SnPO and sSnPO can coordinate water ligands to become hexahedrally or octahedrally coordinated after hydration treatment [73]. This phenomenon can explain why the catalytic activity of calcined SnPO is remarkably higher than SnPO without calcination treatment.

To gain more insight into the activity discrepancy between the three materials, the X-ray photoelectron spectroscopy (XPS) of SnPO, sSnPO and SnO_2 were measured. As shown in Fig. 11a, the XPS spectra of SnO_2 showed binding energies at 494.4 and 486.0 eV, corresponding to the signals of Sn $3d_{3/2}$ and $3d_{5/2}$. This is in accordance with the binding energies reported in the literature for SnO_2 materials [74,75]. The XPS spectra of SnPO and sSnPO displayed signals for Sn $3d_{3/2}$ and $3d_{5/2}$ at 495.8 and 487.5 eV, as are close to the binding energies for other tin phosphate materials reported in previous studies [68,76]. The binding energies of Sn $3d_{3/2}$ and $3d_{5/2}$ in sSnPO and SnPO are slightly higher than that of SnO_2, manifesting the generation of tin species with stronger Lewis acidity [77]. The XPS spectra of sSnPO and SnPO showed a peak at 133.5 eV attributed to the P 2p species, indicating the formation of Sn—O—P bond (Fig. 11b). Moreover, the higher strength of P 2p peak in SnPO also supported that the degree of phosphorylation of SnPO is higher than that of sSnPO.

3.2.3. Acidity properties

The acidic properties of SnO_2, sSnPO and SnPO were investigated by FTIR spectra after pyridine chemisorption, as shown in Fig. 12. According to previous studies, the peaks at 1450, 1576, 1612 cm^{-1} were identified as vibrations characteristic of pyridine sorption on strong Lewis acid sites (denoted with SL), weak Lewis acid sites (WL) and SL, respectively [68]. The generation of Lewis acidity sites is owing to the formation of tetra-coordinated Sn^{4+} site within the SnPO framework [45,68]. The peaks at 1543 and 1637 cm^{-1} were assigned to the adsorbed pyridine at Brønsted acidic sites, and the peak at 1489 cm^{-1} was attributed to the overlap of Brønsted and Lewis acid sites [73]. The concentration of Brønsted (C_B) and Lewis acid sites (C_L) were calculated on the basis of extinction coefficients for bands at 1543 and 1450 cm^{-1} and summarized in Table 3. The concentration of Lewis acid sites increases in the following order: SnO_2 < sSnPO < SnPO, correlating well with their catalytic activity. In contrast, the concentration of Brønsted acid sites increases in the following order: SnPO < SnO_2 < sSnPO. The presence of Brønsted acid in BMIMBr could not only promote the conversion of fructose into HMF but also accelerate the degradation of glucose and HMF into undesirable by-products [44].

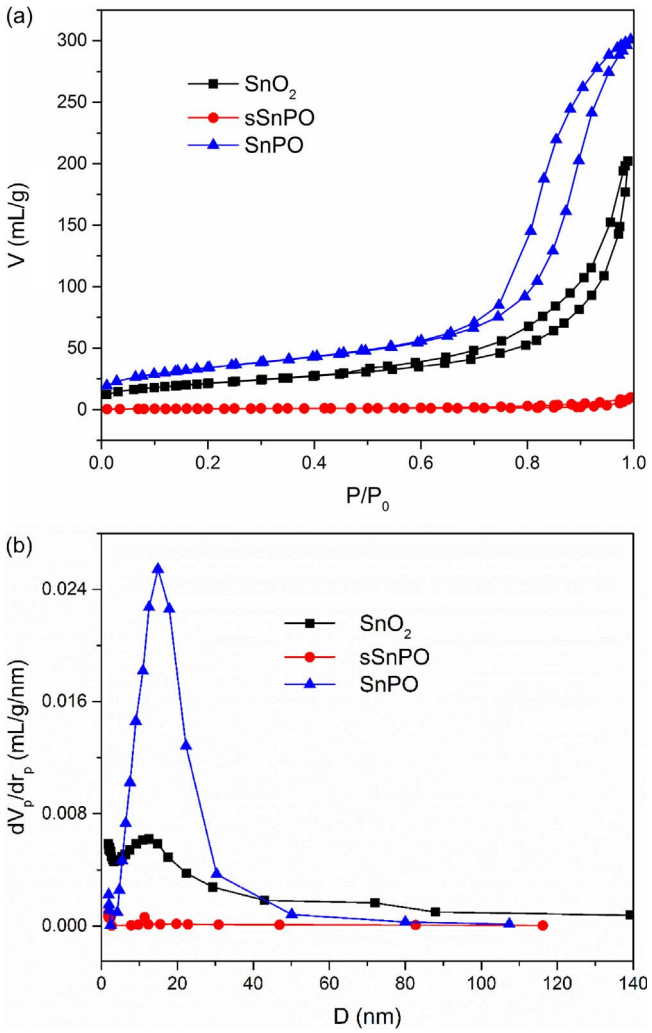

Fig. 7. (a) N_2 adsorption-desorption isotherms and (b) pore size distributions curves of SnO_2, sSnPO and SnPO.

Table 3
Morphology and acid site analysis of SnO_2, sSnPO and SnPO.

Catalyst	S_{BET} ($m^2\ g^{-1}$)	V_{pore} ($cm^3\ g^{-1}$)	D_{meso} (nm)	C_B (μmol g^{-1})	C_L (μmol g^{-1})	C_B/C_L
SnO_2	75.3	0.31	17.7	8.6	26.2	0.32
sSnPO	4.7	0.01	19.7	10.3	62.0	0.16
SnPO	120.8	0.46	15.4	7.6	129.3	0.06

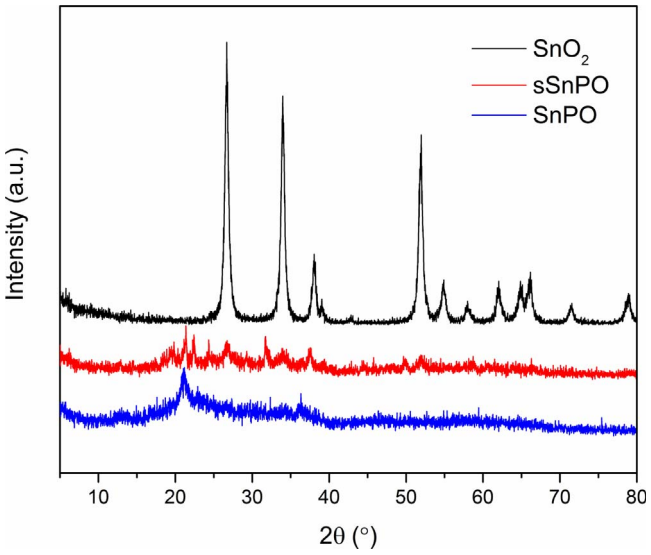

Fig. 8. X-ray diffraction pattern of SnO_2, sSnPO and SnPO.

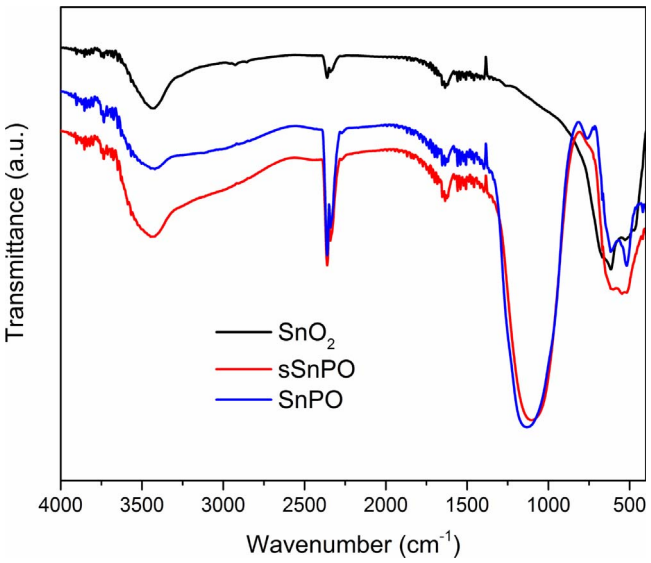

Fig. 9. FTIR spectra of SnPO, sSnPO and SnO_2.

Actually, in BMIMBr, the rate-determining step is the isomerization of glucose into fructose, which is catalyzed by only specific Lewis acid. Therefore, these results indicated the high concentration of Lewis acid sites and low concentration of Brønsted acid sites in SnPO give rise to better catalytic performance for the conversion of glucose to HMF in the SnPO/EMIMBr system.

The nature of Lewis acidic Sn sites in SnO_2, sSnPO and SnPO was further investigated by FTIR measurement with deuterated acetonitrile (CD_3CN). The IR spectra of adsorbed CD_3CN have been widely used to distinguish open Sn and closed Sn sites in Sn-beta zeolite materials [73]. As shown in Fig. 13, the IR spectra for SnO_2, sSnPO and SnPO exposed to CD_3CN all exhibited bands at 2310 and 2320 cm^{-1}, resulting from the CD_3CN coordinated to Lewis acid sites [70]. Combined with the results from diffuse reflectance UV–vis spectra, the bands at 2310 and 2320 cm^{-1} were attributed to closed Sn sites and open Sn sites, respectively [70,73]. The higher intensity of peaks in SnPO indicated that the content of Lewis acid sites in SnPO is higher than the latter two materials, consistent with the pyridine FTIR measurements.

3.3. Reaction pathway for conversion of glucose to HMF

Based on the catalytic study and comprehensive characterization of SnO_2, sSnPO and SnPO, we found that the content of tetra-coordinated Sn^{4+} sites in the catalysts correlates well with their catalytic performance. These results are consistent with previous studies on the isomerization of glucose using other Sn-containing materials, including Sn-beta zeolite, (POSS)-Sn-(POSS) complex grafted on silica and porous tin-organic frameworks [78–80]. Therefore, the tetra-coordinated Sn^{4+} sites in SnPO were identified as the major catalytic species for the isomerization of glucose into fructose [81]. Previous studies have shown that the framework tin sites located within the hydrophobic channels of Sn-beta zeolite are highly active for the isomerization of glucose into fructose in both water and methanol solvent, while SnO_2 particles located at external zeolite crystal surfaces or supported on

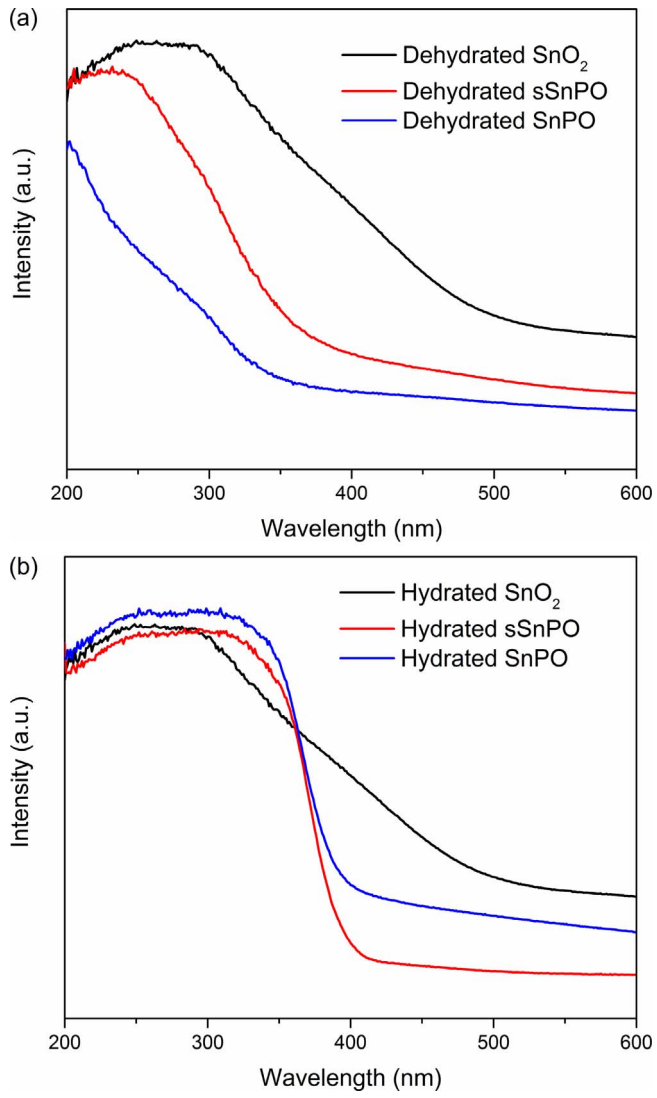

Fig. 10. Diffuse reflectance UV–vis spectra of dehydrated (a) and hydrated (b) SnPO, sSnPO and SnO_2.

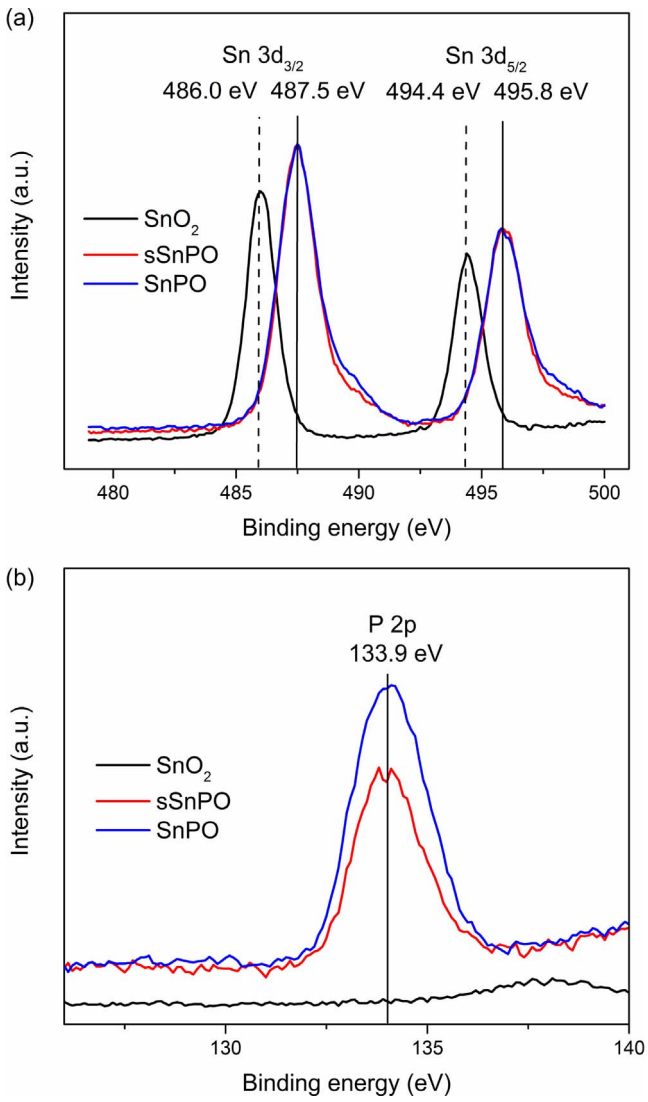

Fig. 11. XPS spectra of Sn 3d (a), P 2p (b) of SnPO, sSnPO and SnO_2.

amorphous silica catalyze isomerization in methanol, but not in water [59,60,81,82]. In the present work, we have demonstrated that the tetrahedrally coordinated Sn^{4+} sites in SnPO are very active for isomerization of glucose into fructose in EMIMBr, not in water. These results suggest that the tetrahedrally coordinated Sn^{4+} sites are effective for glucose isomerization in anhydrous environmental.

Besides, we have demonstrated that ionic liquid EMIMBr could catalyze the conversion of fructose into HMF almost quantitatively, with a reaction rate higher than the isomerization of glucose to fructose [55]. Therefore, a reaction pathway of glucose in the EMIMBr/SnPO system was proposed: SnPO first catalyzes the isomerization of glucose into fructose and then the formed fructose can be immediately converted into HMF by EMIMBr. Although the efficiency and selectivity of glucose isomerization into fructose in water is usually low, the instantaneous consumption of fructose in EMIMBr could shift the reaction equilibrium and promote the isomerization of glucose into fructose. Through this mechanism, high concentration-glucose could be efficiently converted to HMF with high selectivity. These results suggest that the superior catalytic performance of the SnPO/EMIMBr system is due to the synergistic effect between SnPO and EMIMBr. As an example, our work demonstrates that the combined use of heterogeneous catalyst and ionic liquid is an effective strategy to enhance the conversion of glucose to HMF. Therefore, the systematic investigation on other catalysts and solvents should open opportunities of innovation for cost-effective HMF production from biomass.

4. Conclusion

A series of metal oxides and metal phosphates was screened as heterogeneous catalysts for the conversion of glucose into HMF in EMIMBr. It was found that tin phosphate can convert a high-concentration of glucose (10 wt%) into HMF with a yield (58.3%) comparable to the best results obtained with the most active homogeneous catalysts. Detailed characterizations of catalyst and control experiments were performed to elucidate the reaction mechanism. Tetra-coordinated Sn^{4+} sites from tin phosphate were identified as the major catalytic species for the isomerization of glucose into fructose. The high yield of HMF was attributed to the synergistic effect between SnPO and EMIMBr.

Acknowledgements

This work was supported by the International Joint Research Projects in the Science & Technology Pillar Program of Tianjin, China (13RCGFSF14300), Research Projects in the Science & Technology Pillar Program of Tianjin, China (14TXGCCX00012), Research Projects

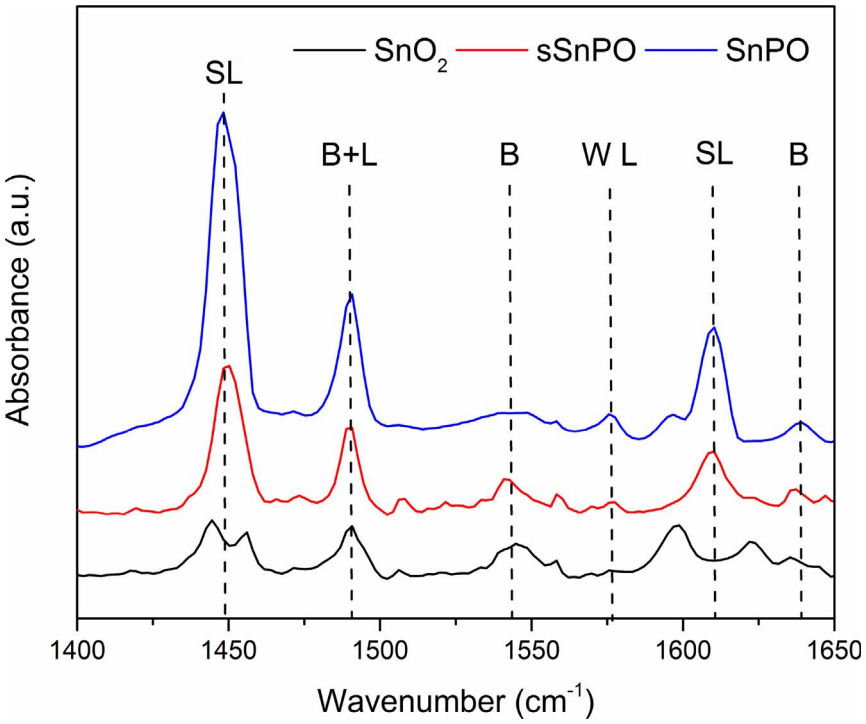

Fig. 12. FTIR difference spectra of SnO_2, sSnPO and SnPO exposed to pyridine.

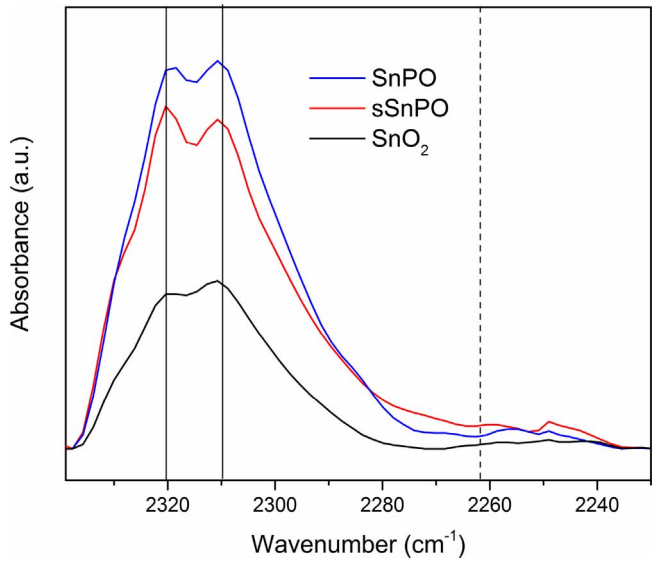

Fig. 13. FTIR difference spectra of SnO_2, sSnPO and SnPO exposed to CD_3CN.

in the Science & Technology Program of Jinnan District Tianjin, China (2015JNKW0005), Research Projects in the Science & Technology Pillar Program of Tianjin, China (15JCTPJC63300), Research Projects in the Science & Technology Pillar Program of Tianjin, China (17JCZDJC39500) and Project supported by the National Science Foundation for Young Scientists of China (51708301).

References

[1] L. Negahdar, I. Delidovich, R. Palkovits, Aqueous-phase hydrolysis of cellulose and hemicelluloses over molecular acidic catalysts: insights into the kinetics and reaction mechanism, Appl. Catal. B 184 (2016) 285–298.
[2] S. Eibner, A. Margeriat, F. Broust, D. Laurenti, C. Geantet, A. Julbe, J. Blin, Catalytic deoxygenation of model compounds from flash pyrolysis of lignocellulosic biomass over activated charcoal-based catalysts, Appl. Catal. B 219 (2017) 517–525.
[3] Y. Yao, C. Lian, G. Wu, Y. Hu, F. Wei, M. Yu, S. Wang, Synthesis of sea urchin-like carbon nanotubes/porous carbon superstructures derived from waste biomass for treatment of various contaminants, Appl. Catal. B 219 (2017) 563–571.
[4] L.S. Ribeiro, J.J. Delgado, J.J.M. Órfão, M.F.R. Pereira, Carbon supported Ru-Ni bimetallic catalysts for the enhanced one-pot conversion of cellulose to sorbitol, Appl. Catal. B 217 (2017) 265–274.
[5] M. Oregui-Bengoechea, I. Gandarias, N. Miletić, S.F. Simonsen, A. Kronstad, P.L. Arias, T. Barth, Thermocatalytic conversion of lignin in an ethanol/formic acid medium with NiMo catalysts: role of the metal and acid sites, Appl. Catal. B 217 (2017) 353–364.
[6] M. Yabushita, H. Kobayashi, A. Fukuoka, Catalytic transformation of cellulose into platform chemicals, Appl. Catal. B 145 (2014) 1–9.
[7] R.F. Cotta, K.A. da Silva Rocha, E.F. Kozhevnikova, I.V. Kozhevnikov, E.V. Gusevskaya, Heteropoly acid catalysts in upgrading of biorenewables: cycloaddition of aldehydes to monoterpenes in green solvents, Appl. Catal. B 217 (2017) 92–99.
[8] I. Rossetti, M. Compagnoni, E. Finocchio, G. Ramis, A. Di Michele, Y. Millot, S. Dzwigaj, Ethylene production via catalytic dehydration of diluted bioethanol: a step towards an integrated biorefinery, Appl. Catal. B 210 (2017) 407–420.
[9] H. Li, Z. Fang, J. Luo, S. Yang, Direct conversion of biomass components to the biofuel methyl levulinate catalyzed by acid-base bifunctional zirconia-zeolites, Appl. Catal. B 200 (2017) 182–191.
[10] S.D. Stefanidis, S.A. Karakoulia, K.G. Kalogiannis, E.F. Iliopoulou, A. Delimitis, H. Yiannoulakis, T. Zampetakis, A.A. Lappas, K.S. Triantafyllidis, Natural magnesium oxide (MgO) catalysts: a cost-effective sustainable alternative to acid zeolites for the in situ upgrading of biomass fast pyrolysis oil, Appl. Catal. B 196 (2016) 155–173.
[11] S. Kelkar, C.M. Saffron, K. Andreassi, Z. Li, A. Murkute, D.J. Miller, T.J. Pinnavaia, R.M. Kriegel, A survey of catalysts for aromatics from fast pyrolysis of biomass, Appl. Catal. B 174 (2015) 85–95.
[12] L.J. Konwar, P. Mäki-Arvela, E. Salminen, N. Kumar, A.J. Thakur, J.-P. Mikkola, D. Deka, Towards carbon efficient biorefining: multifunctional mesoporous solid acids obtained from biodiesel production wastes for biomass conversion, Appl. Catal. B 176 (2015) 20–35.
[13] B.M. Matsagar, P.L. Dhepe, Bronsted acidic ionic liquid-catalyzed conversion of hemicellulose into sugars, Catal. Sci. Technol. 5 (2015) 531–539.
[14] B.M. Matsagar, P.L. Dhepe, Effects of cations, anions and H^+ concentration of acidic ionic liquids on the valorization of polysaccharides into furfural, New J. Chem. 41 (2017) 6137–6144.
[15] Q. Hou, W. Li, M. Ju, L. Liu, Y. Chen, Q. Yang, J. Wang, Separation of polysaccharides from rice husk and wheat bran using solvent system consisting of BMIMOAc and DMI, Carbohydr. Polym. 133 (2015) 517–523.
[16] L. Da Vià, C. Recchi, E.O. Gonzalez-Yañez, T.E. Davies, J.A. Lopez-Sanchez, Visible light selective photocatalytic conversion of glucose by TiO_2, Appl. Catal. B 202 (2017) 281–288.
[17] K. Morawa Eblagon, M.F.R. Pereira, J.L. Figueiredo, One-pot oxidation of cellobiose to gluconic acid. Unprecedented high selectivity on bifunctional gold catalysts over mesoporous carbon by integrated texture and surface chemistry optimization, Appl. Catal. B 184 (2016) 381–396.
[18] L. Hu, L. Lin, Z. Wu, S. Zhou, S. Liu, Chemocatalytic hydrolysis of cellulose into glucose over solid acid catalysts, Appl. Catal. B 174–175 (2015) 225–243.

[19] H. Li, W. Zhao, Z. Fang, Hydrophobic Pd nanocatalysts for one-pot and high-yield production of liquid furanic biofuels at low temperatures, Appl. Catal. B 215 (2017) 18–27.
[20] B. Liu, Z. Zhang, Catalytic conversion of biomass into chemicals and fuels over magnetic catalysts, ACS Catal. 6 (2016) 326–338.
[21] K. Yan, Y. Yang, J. Chai, Y. Lu, Catalytic reactions of gamma-valerolactone: a platform to fuels and value-added chemicals, Appl. Catal. B 179 (2015) 292–304.
[22] J. Cueto, L. Faba, E. Díaz, S. Ordóñez, Performance of basic mixed oxides for aqueous-phase 5-hydroxymethylfurfural-acetone aldol condensation, Appl. Catal. B 201 (2017) 221–231.
[23] Q. Meng, D. Cao, G. Zhao, C. Qiu, X. Liu, X. Wen, Y. Zhu, Y. Li, The role of water on the selective decarbonylation of 5-hydroxymethylfurfural over Pd/Al_2O_3 catalyst: experimental and DFT studies, Appl. Catal. B 212 (2017) 15–22.
[24] I. Obregón, I. Gandarias, A. Ocio, I. García-García, N. Alvarez de Eulate, P.L. Arias, Structure-activity relationships of Ni-Cu/Al_2O_3 catalysts for γ-valerolactone conversion to 2-methyltetrahydrofuran, Appl. Catal. B 210 (2017) 328–341.
[25] Y. Yan, K. Li, J. Zhao, W. Cai, Y. Yang, J.-M. Lee, Nanobelt-arrayed vanadium oxide hierarchical microspheres as catalysts for selective oxidation of 5-hydroxymethylfurfural toward 2, 5-diformylfuran, Appl. Catal. B 207 (2017) 358–365.
[26] B. Chen, F. Li, Z. Huang, G. Yuan, Carbon-coated Cu-Co bimetallic nanoparticles as selective and recyclable catalysts for production of biofuel 2, 5-dimethylfuran, Appl. Catal. B 200 (2017) 192–199.
[27] J. Luo, J.D. Lee, H. Yun, C. Wang, M. Monai, C.B. Murray, P. Fornasiero, R.J. Gorte, Base metal-Pt alloys: a general route to high selectivity and stability in the production of biofuels from HMF, Appl. Catal. B 199 (2016) 439–446.
[28] T.-W. Kim, S.-Y. Kim, J.-C. Kim, Y. Kim, R. Ryoo, C.-U. Kim, Selective p-xylene production from biomass-derived dimethylfuran and ethylene over zeolite beta nanosponge catalysts, Appl. Catal. B 185 (2016) 100–109.
[29] A. Gelmini, S. Albonetti, F. Cavani, C. Cesari, A. Lolli, V. Zanotti, R. Mazzoni, Oxidant free one-pot transformation of bio-based 2, 5-bis-hydroxymethylfuran into α-6-hydroxy-6-methyl-4-enyl-2H-pyran-3-one in water, Appl. Catal. B 180 (2016) 38–43.
[30] S. Albonetti, A. Lolli, V. Morandi, A. Migliori, C. Lucarelli, F. Cavani, Conversion of 5-hydroxymethylfurfural to 2, 5-furandicarboxylic acid over Au-based catalysts: optimization of active phase and metal-support interaction, Appl. Catal. B 163 (2015) 520–530.
[31] F. Neaţu, R.S. Marin, M. Florea, N. Petrea, O.D. Pavel, V.I. Pârvulescu, Selective oxidation of 5-hydroxymethyl furfural over non-precious metal heterogeneous catalysts, Appl. Catal. B 180 (2016) 751–757.
[32] A. Banerjee, G.R. Dick, T. Yoshino, M.W. Kanan, Carbon dioxide utilization via carbonate-promoted C-H carboxylation, Nature 531 (2016) 215–219.
[33] I. Krivtsov, E.I. García-López, G. Marcì, L. Palmisano, Z. Amghouz, J.R. García, S. Ordóñez, E. Díaz, Selective photocatalytic oxidation of 5-hydroxymethyl-2-furfural to 2, 5-furandicarboxyaldehyde in aqueous suspension of g-C_3N_4, Appl. Catal. B 204 (2017) 430–439.
[34] Z. Zhang, J. Song, B. Han, Catalytic transformation of lignocellulose into chemicals and fuel products in ionic liquids, Chem. Rev. 117 (2017) 6834–6880.
[35] X. Zhang, K. Wilson, A.F. Lee, Heterogeneously catalyzed hydrothermal processing of C_5-C_6 sugars, Chem. Rev. 116 (2016) 12328–12368.
[36] H. Zhao, J.E. Holladay, H. Brown, Z.C. Zhang, Metal chlorides in ionic liquid solvents convert sugars to 5-hydroxymethylfurfural, Science 316 (2007) 1597–1600.
[37] J. Zhou, Z. Xia, T. Huang, P. Yan, W. Xu, Z. Xu, J. Wang, Z.C. Zhang, An ionic liquid-organics-water ternary biphasic system enhances the 5-hydroxymethylfurfural yield in catalytic conversion of glucose at high concentrations, Green Chem. 17 (2015) 4206–4216.
[38] J.B. Binder, R.T. Raines, Simple chemical transformation of lignocellulosic biomass into furans for fuels and chemicals, J. Am. Chem. Soc. 131 (2009) 1979–1985.
[39] Y.J. Pagán-Torres, T. Wang, J.M.R. Gallo, B.H. Shanks, J.A. Dumesic, Production of 5-hydroxymethylfurfural from glucose using a combination of lewis and brønsted acid catalysts in water in a biphasic reactor with an alkylphenol solvent, ACS Catal. 2 (2012) 930–934.
[40] M.E. Zakrzewska, E. Bogel-Łukasik, R. Bogel-Łukasik, Ionic liquid-mediated formation of 5-hydroxymethylfurfural-a promising biomass-derived building block, Chem. Rev. 111 (2011) 397–417.
[41] S. Jia, Z. Xu, Z. Zhang, Catalytic conversion of glucose in dimethylsulfoxide/water binary mix with chromium trichloride: role of water on the product distribution, Chem. Eng. J. 254 (2014) 333–339.
[42] J. Tang, L. Zhu, X. Fu, J. Dai, X. Guo, C. Hu, Insights into the kinetics and reaction network of aluminum chloride-catalyzed conversion of glucose in NaCl-H_2O/THF biphasic system, ACS Catal. (2017) 256–266.
[43] Z. Zhang, M. Sadakane, N. Hiyoshi, A. Yoshida, M. Hara, W. Ueda, Acidic ultrafine tungsten oxide molecular wires for cellulosic biomass conversion, Angew. Chem. Int. Ed. 55 (2016) 10234–10238.
[44] P. Carniti, A. Gervasini, F. Bossola, V. Dal Santo, Cooperative action of Brønsted and Lewis acid sites of niobium phosphate catalysts for cellobiose conversion in water, Appl. Catal. B 193 (2016) 93–102.
[45] V.V. Ordomsky, V.L. Sushkevich, J.C. Schouten, J. Van Der Schaaf, T.A. Nijhuis, Glucose dehydration to 5-hydroxymethylfurfural over phosphate catalysts, J. Catal. 300 (2013) 37–46.
[46] I. Jiménez-Morales, J. Santamaría-González, A. Jiménez-López, P. Maireles-Torres, Glucose dehydration to 5-hydroxymethylfurfural on zirconium containing mesoporous MCM-41 silica catalysts, Fuel 118 (2014) 265–271.
[47] B. Saha, M.M. Abu-Omar, Advances in 5-hydroxymethylfurfural production from biomass in biphasic solvents, Green Chem. 16 (2014) 24–38.
[48] I. Graça, D. Iruretagoyena, D. Chadwick, Glucose isomerisation into fructose over magnesium-impregnated NaY zeolite catalysts, Appl. Catal. B 206 (2017) 434–443.
[49] I. Delidovich, R. Palkovits, Fructose production via extraction-assisted isomerization of glucose catalyzed by phosphates, Green Chem. 18 (2016) 5822–5830.
[50] C. Antonetti, M. Melloni, D. Licursi, S. Fulignati, E. Ribechini, S. Rivas, J.C. Parajó, F. Cavani, A.M. Raspolli Galletti, Microwave-assisted dehydration of fructose and inulin to HMF catalyzed by niobium and zirconium phosphate catalysts, Appl. Catal. B 206 (2017) 364–377.
[51] K. Tsutsumi, N. Kurata, E. Takata, K. Furuichi, M. Nagano, K. Tabata, Silicon semiconductor-assisted Brønsted acid-catalyzed dehydration: highly selective synthesis of 5-hydroxymethylfurfural from fructose under visible light irradiation, Appl. Catal. B 147 (2014) 1009–1014.
[52] J. Zhang, A. Das, R.S. Assary, L.A. Curtiss, E. Weitz, A combined experimental and computational study of the mechanism of fructose dehydration to 5-hydroxymethylfurfural in dimethylsulfoxide using Amberlyst 70, PO_4^{3-}/niobic acid, or sulfuric acid catalysts, Appl. Catal. B 181 (2016) 874–887.
[53] Q. Hou, W. Li, M. Ju, L. Liu, Y. Chen, Q. Yang, One-pot synthesis of sulfonated graphene oxide for efficient conversion of fructose into HMF, RSC Adv. 6 (2016) 104016–104024.
[54] B.M. Matsagar, M.K. Munshi, A.A. Kelkar, P.L. Dhepe, Conversion of concentrated sugar solutions into 5-hydroxymethyl furfural and furfural using Bronsted acidic ionic liquids, Catal. Sci. Technol. 5 (2015) 5086–5090.
[55] Y.N. Li, J.Q. Wang, L.N. He, Z.Z. Yang, A.H. Liu, B. Yu, C.R. Luan, Experimental and theoretical studies on imidazolium ionic liquid-promoted conversion of fructose to 5-hydroxymethylfurfural, Green Chem. 14 (2012) 2752–2758.
[56] A. Dutta, D. Gupta, A.K. Patra, B. Saha, A. Bhaumik, Synthesis of 5-hydroxymethylfurural from carbohydrates using large-pore mesoporous tin phosphate, ChemSusChem 7 (2014) 925–933.
[57] F. Li, L.J. France, Z. Cai, Y. Li, S. Liu, H. Lou, J. Long, X. Li, Catalytic transfer hydrogenation of butyl levulinate to γ-valerolactone over zirconium phosphates with adjustable Lewis and Brønsted acid sites, Appl. Catal. B 214 (2017) 67–77.
[58] H. Li, W. Xu, T. Huang, S. Jia, Z. Xu, P. Yan, X. Liu, Z.C. Zhang, Distinctive aldose isomerization characteristics and the coordination chemistry of metal chlorides in 1-butyl-3-methylimidazolium chloride, ACS Catal. 4 (2014) 4446–4454.
[59] M. Moliner, Y. Román-Leshkov, M.E. Davis, Tin-containing zeolites are highly active catalysts for the isomerization of glucose in water, Proc. Natl. Acad. Sci. U. S. A. 107 (2010) 6164–6168.
[60] R. Bermejo-Deval, R. Gounder, M.E. Davis, Framework and extraframework tin sites in zeolite beta react glucose differently, ACS Catal. 2 (2012) 2705–2713.
[61] E. Nikolla, Y. Román-Leshkov, M. Moliner, M.E. Davis, One-pot synthesis of 5-(hydroxymethyl)furfural from carbohydrates using tin-beta zeolite, ACS Catal. 1 (2011) 408–410.
[62] J. Guo, S. Zhu, Y. Cen, Z. Qin, J. Wang, W. Fan, Ordered mesoporous Nb-W oxides for the conversion of glucose to fructose, mannose and 5-hydroxymethylfurfural, Appl. Catal. B 200 (2017) 611–619.
[63] C. García-Sancho, I. Fúnez-Núñez, R. Moreno-Tost, J. Santamaría-González, E. Pérez-Inestrosa, J.L.G. Fierro, P. Maireles-Torres, Beneficial effects of calcium chloride on glucose dehydration to 5-hydroxymethylfurfural in the presence of alumina as catalyst, Appl. Catal. B 206 (2017) 617–625.
[64] I. Jiménez-Morales, A. Teckchandani-Ortiz, J. Santamaría-González, P. Maireles-Torres, A. Jiménez-López, Selective dehydration of glucose to 5-hydroxymethylfurfural on acidic mesoporous tantalum phosphate, Appl. Catal. B 144 (2014) 22–28.
[65] I. Jiménez-Morales, M. Moreno-Recio, J. Santamaría-González, P. Maireles-Torres, A. Jiménez-López, Mesoporous tantalum oxide as catalyst for dehydration of glucose to 5-hydroxymethylfurfural, Appl. Catal. B 154–155 (2014) 190–196.
[66] I. Jiménez-Morales, M. Moreno-Recio, J. Santamaría-González, P. Maireles-Torres, A. Jiménez-López, Production of 5-hydroxymethylfurfural from glucose using aluminium doped MCM-41 silica as acid catalyst, Appl. Catal. B 164 (2015) 70–76.
[67] R. Noma, K. Nakajima, K. Kamata, M. Kitano, S. Hayashi, M. Hara, Formation of 5-(hydroxymethyl)furfural by stepwise dehydration over TiO_2; with water-tolerant Lewis acid sites, J. Phys. Chem. C 119 (2015) 17117–17125.
[68] X. Wang, F. Liang, C. Huang, Y. Li, B. Chen, Highly active tin(iv) phosphate phase transfer catalysts for the production of lactic acid from triose sugars, Catal. Sci. Technol. 5 (2015) 4410–4421.
[69] J. Dijkmans, J. Demol, K. Houthoofd, S. Huang, Y. Pontikes, B. Sels, Post-synthesis Snβ. An exploration of synthesis parameters and catalysis, J. Catal. 330 (2015) 545–557.
[70] J. Dijkmans, M. Dusselier, D. Gabriëls, K. Houthoofd, P.C.M.M. Magusin, S. Huang, Y. Pontikes, M. Trekels, A. Vantomme, L. Giebeler, S. Oswald, B.F. Sels, Cooperative catalysis for multistep biomass conversion with Sn/Al beta zeolite, ACS Catal. 5 (2015) 928–940.
[71] N.K. Mal, S. Ichikawa, M. Fujiwara, Synthesis of a novel mesoporous tin phosphate, $SnPO_4$, Chem. Commun. (2002) 112–113.
[72] X. Yang, J. Bian, J. Huang, W. Xin, T. Lu, C. Chen, Y. Su, L. Zhou, F. Wang, J. Xu, Fluoride-free and low concentration template synthesis of hierarchical Sn-Beta zeolites: efficient catalysts for conversion of glucose to alkyl lactate, Green Chem. 19 (2017) 692–701.
[73] J.W. Harris, M.J. Cordon, J.R. Di Iorio, J.C. Vega-Vila, F.H. Ribeiro, R. Gounder, Titration and quantification of open and closed Lewis acid sites in Sn-Beta zeolites that catalyze glucose isomerization, J. Catal. 335 (2016) 141–154.
[74] C. Wang, J. Li, Y. Zhang, Y. Wei, J. Liu, The influence of phosphate on crystal grain growth of nanosized SnO_2, J. Alloys Compd. 493 (2010) 64–69.
[75] Y. Sun, F. Lei, S. Gao, B. Pan, J. Zhou, Y. Xie, Atomically thin tin dioxide sheets for efficient catalytic oxidation of carbon monoxide, Angew. Chem. Int. Ed. 52 (2013) 10569–10572.
[76] M. Pramanik, J. Lee, S. Tominaka, Y. Ide, J.H. Kim, Y. Yamauchi, Unique nanocrystalline frameworks in mesoporous tin phosphate prepared through a

hydrofluoric acid assisted chemical reaction, J. Mater. Chem. A 4 (2016) 18091–18099.
[77] H. Li, J. He, A. Riisager, S. Saravanamurugan, B. Song, S. Yang, Acid–base bifunctional zirconium N-alkyltriphosphate nanohybrid for hydrogen transfer of biomass-derived carboxides, ACS Catal. 6 (2016) 7722–7727.
[78] P. Ferrini, J. Dijkmans, R. De Clercq, S. Van de Vyver, M. Dusselier, P.A. Jacobs, B.F. Sels, Lewis acid catalysis on single site Sn centers incorporated into silica hosts, Coord. Chem. Rev. 343 (2017) 220–255.
[79] E.V. Beletskiy, X. Hou, Z. Shen, J.R. Gallagher, J.T. Miller, Y. Wu, T. Li, M.C. Kung, H.H. Kung, Supported tetrahedral oxo-Sn catalyst: single site two modes of catalysis, J. Am. Chem. Soc. 138 (2016) 4294–4297.
[80] I. Delidovich, A. Hoffmann, A. Willms, M. Rose, Porous tin-organic frameworks as selective epimerization catalysts in aqueous solutions, ACS Catal. 7 (2017) 3792–3798.
[81] Y. Román-Leshkov, M. Moliner, J.A. Labinger, M.E. Davis, Mechanism of glucose isomerization using a solid lewis acid catalyst in water, Angew. Chem. Int. Ed. 49 (2010) 8954–8957.
[82] S. Saravanamurugan, M. Paniagua, J.A. Melero, A. Riisager, Efficient isomerization of glucose to fructose over zeolites in consecutive reactions in alcohol and aqueous media, J. Am. Chem. Soc. 135 (2013) 5246–5249.